0287-F

# FREQUENCY AGILE MATERIALS FOR ELECTRONICS (FAME)
# Final Report

Prepared by

Brian Moeckly
**Conductus, Inc.**
460 Ward Drive
Santa Barbara, CA 93111-2310

August 7, 1998 through February 28, 2003

**Contract N00014-98-C-0287**

Prepared for
**Office of Naval Research**
Ballston Tower One
800 North Quincy Street
Arlington, VA 22217-5660

DISTRIBUTION STATEMENT A
Approved for Public Release
Distribution Unlimited

The views and conclusions contained in this document are those of the author and should not be interpreted as necessarily representing the official policies, either expressed or implied, of the Advanced Research Projects Agency of the U.S. Government.

# REPORT DOCUMENTATION PAGE

*Form Approved*
*OMB No. 0704-0188*

Public reporting burden for this collection of information is estimated to average 1 hour per response, including the time for reviewing instructions, searching existing data sources, gathering and maintaining the data needed, and completing and reviewing the collection of information. Send comments regarding this burden estimate or any other aspect of this collection of information, including suggestions for reducing this burden, to Washington Headquarters Services, Directorate for Information Operations and Reports, 1215 Jefferson Davis Highway, Suite 1204, Arlington, VA 22202-4302, and to the Office of Management and Budget, Paperwork Reduction Project (0704-0188), Washington, DC 20503.

| 1. AGENCY USE ONLY *(Leave blank)* | 2. REPORT DATE | 3. REPORT TYPE AND DATES COVERED |
|---|---|---|
| | November 30, 2004 | Final Report 8/7/98 – 2/28/03 |

**4. TITLE AND SUBTITLE**
Frequency Agile Materials for Electronics (FAME) Final Report

**5. FUNDING NUMBERS**
N00014-98-C-0287

**6. AUTHORS**
Brian Moeckly

**7. PERFORMING ORGANIZATION NAME(S) AND ADDRESS(ES)**
Conductus, Inc.
460 Ward Drive
Santa Barbara, CA 93111

**8. PERFORMING ORGANIZATION REPORT NUMBER**
0287-F

**9. SPONSORING/MONITORING AGENCY NAME(S) AND ADDRESS(ES)**
Office of Naval Research
Ballston Tower One
800 North Quincy Street
Arlington, VA 22217-5660

**10. SPONSORING/MONITORING AGENCY REPORT NUMBER**
CLIN 0004

**11. SUPPLEMENTARY NOTES**

**12a. DISTRIBUTION/AVAILABILITY STATEMENT**
Approved for public release; distribution is unlimited

**12b. DISTRIBUTION CODE**
A

**13. ABSTRACT** *(Maximum 200 words)*

High performance HTS microwave filters stand to benefit from the capability to electrically tune their frequency of operation. This function may be performed with electric-field tunable dielectric materials such as $SrTiO_3$ (STO). We have optimized the growth of STO thin films for this purpose using the growth techniques of pulsed laser ablation and reactive coevaporation. We have achieved loss tangents on the order of 0.001 at 65 K for these materials, while maintaining acceptable tunability. We have further optimized the design of STO thin-film capacitors, and we have integrated these structures into specially-designed lumped-element $YBa_2Cu_3O_{7-\delta}$ (YBCO) microwave resonators and filters in order to tune their center frequencies. In this report we briefly summarize our materials development efforts as well as the design and performance of frequency agile thin-film HTS resonators and filters. This project culminated in the demonstration of a stand-alone electrically tunable 6-pole HTS filter.

**14. SUBJECT TERMS**
frequency agile, tunable dielectrics, nonlinear ferroelectrics, strontium titanate, superconductive filters, tunable microwave filters, HTS thin films, pulsed laser ablation, reactive coevaporation, RHEED

**15. NUMBER OF PAGES**
30

**16. PRICE CODE**

| 17. SECURITY CLASSIFICATION OF REPORT | 18. SECURITY CLASSIFICATION OF THIS PAGE | 19. SECURITY CLASSIFICATION OF ABSTRACT | 20. LIMITATION OF ABSTRACT |
|---|---|---|---|
| U | U | U | U |

# FREQUENCY AGILE MATERIALS FOR ELECTRONICS (FAME)
## Final Report

August 7, 1998 through February 28, 2003

## Summary

The broad goals of this program were: a) the development of electric-field tunable dielectric thin films operating at cryogenic temperatures; b) the study of the loss, tunability, and RF properties of these films; and c) the design, evaluation, and optimization of electric-field tunable HTS thin-film microwave resonators and filters that incorporate our tunable dielectric materials. These three goals were synthesized in the development of a stand-alone 6-pole electrically tunable HTS filter.

This program saw demonstration of the following:

- We grew high quality STO films with excellent tunability.
- We reported record dielectric constant values for heteroepitaxial STO films.
- We studied the growth of these materials by pulsed laser deposition, including examination of growth conditions, substrates and substrate surface preparation, film thickness, elemental doping, oxygen and ozone annealing, the use buffer layers, the growth of superlattice structures, and the use of different targets in order to optimize the properties of these films.
- We developed a manufacturable process for large-area deposition of STO films using the technique of reactive coevaporation. The films were optimized by studying the effects of growth conditions, composition, and deposition rate.
- We developed an *in-situ* RHEED technique for studying the growth of the films, including strain relaxation. *In-situ* RHEED was additionally used as a composition monitoring tool to optimize the growth of these films.
- We optimized STO interdigitated capacitor geometries to minimize the effective loss.
- We characterized our STO films using XRD, AFM, low-frequency measurements, and high-frequency coplanar waveguide measurements.
- We examined several different implementation approaches for incorporation of STO films with YBCO microwave resonators and filters.
- We designed and demonstrated high-performance tunable HTS resonator circuits, for different types of resonators with center frequencies ranging from a few hundred MHz to many GHz. We evaluated the tuning speed of these electrically-tunable circuits.
- We designed and demonstrated two-pole and six-pole tunable HTS filters.

## Introduction

Tunable RF components are desired for their ability to enhance the capability of advanced communications systems. Such tuning is achievable using electric-field-tunable dielectric thin films such as $SrTiO_3$ (STO), and is attractive for a variety of advanced wireless applications. Examples include matching networks, automatic gain controls, time delay devices, phase shifting antenna arrays, and voltage controlled oscillators in phase locked loops. Such technologies can enable interference protection of present communications systems, phased array radar, and wideband multi-channel communications.

Particularly compelling applications also include fixed-frequency technologies such as HTS microwave filters for mobile communications, which will benefit from the elimination of mechanical tuning. For these filters, the stringent requirement of a high quality factor ($Q$) may be balanced by the need for relatively little tuning. STO thin films appear ideal for this purpose. They are compatible with YBCO (as illustrated in Figure 1), and they have a high dielectric constant, hence reducing the required size of tuning elements. Their comparatively high loss tangent is accompanied by a large tunability, i.e., by a large change in their dielectric constant and loss tangent with applied electric field.

Our efforts were to produce STO films with as low loss as possible while maintaining acceptable tunability. However, the loss is still sufficiently high that integration with high-$Q$ materials such as superconductors readily limits their performance. Hence design schemes that optimize the tradeoff between tunability and loss remain necessary, and we will discuss our success at fabricating tunable thin-film HTS resonators and filters.

This report will present the highlights of the results achieved during performance of this FAME program; additional details may be found in previous technical reports and publications.

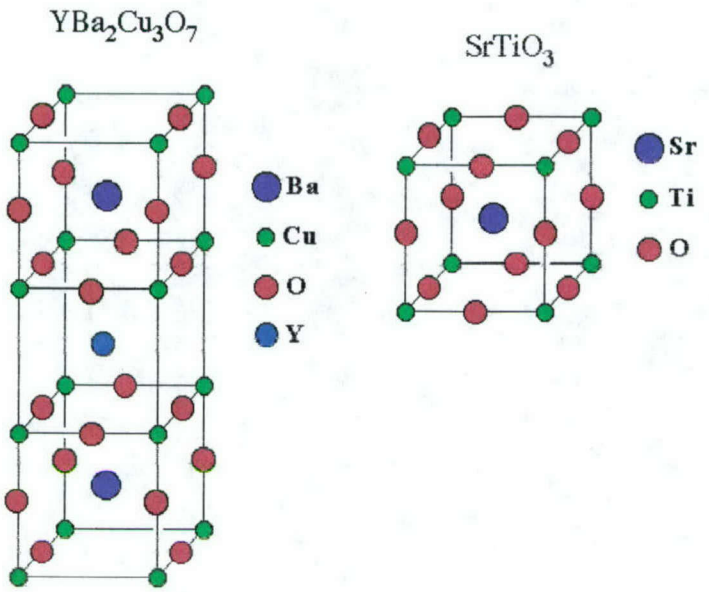


Figure 1. The similarity in crystal structure of YBCO and STO. The distorted YBCO perovskite structure can be viewed as "missing" oxygen atoms which are present in the ideal perovskite structure of STO.

## Technical Problem

The goal of our FAME program was to develop tunable dielectric thin films, to understand their RF properties, and to implement them into advanced superconducting RF circuits. Conductus' expertise is in the development and manufacture of HTS microwave receiver front ends for mobile communications. These circuits derive their outstanding filter properties and low noise from the high $Q$ values afforded by the superconducting filters which operate at cryogenic temperatures. These thin film HTS filters must at present be mechanically tuned in order to adjust the center frequencies of each resonator (typically, up to 10 resonators in one HTS filter), and, once tuned, they operate at fixed frequency. It is highly desirable to realize the implementation of electrically tunable filters with no mechanically moving parts. Such filters would offer the further advantage of being tunable at any time, so that they are field-configurable and so that they can enable a host of tunable RF applications as discussed above.

Electric-field-tunable dielectric materials such as STO would appear to be ideal candidates for this purpose, because their dielectric constant may be altered by applying an electric field. Capacitor structures of these thin film materials can therefore be made and incorporated into HTS filter circuits in order to change the capacitance of the circuits and hence their center frequencies. However, STO suffers from the disadvantage of having a relatively high loss tangent, $\tan\delta$, which, if sufficiently high, can load the HTS circuit and thereby degrade its $Q$ and inherent performance advantage. In general, the loss $Q_{TD}$ in a high-frequency resonator due to a tunable dielectric (TD) is given by

$$1/Q_{TD} = h \tan\delta,$$

where $h$ is a filling factor in the dielectric which relates the center frequency change to that of the dielectric constant change, or

$$\Delta f \sim h\, \Delta\varepsilon$$
$$h = -2(\Delta f/f)/(\Delta\varepsilon/\varepsilon),$$

where $\tan\delta$ is the intrinsic dielectric loss. Hence we observe that that there exists a tradeoff between tunability and $Q$. The design requirement of the filter circuit is to maximize the frequency tunability $\Delta f/f$ while maintaining high $Q$, and it can be seen that this is related to the materials requirement, expressed as an intrinsic figure of merit, $k$, as

$$k = \Delta\varepsilon/(\varepsilon \tan\delta).$$

The goal of the materials development portion of his program is to optimize $k$, and the circuit design requirement is to optimize $\Delta f/f$ while maintaining an acceptably high $Q$.

## General Methodology

This program was structured to achieve the above goals by the following series of sub-projects:

- Growth and optimization of $SrTiO_3$ thin films
  - Pulsed laser deposition (PLD)
  - Reactive coevaporation (RCE)
- Study of the low- and high-frequency dielectric properties of these films
- Correlation of the structural properties with microwave losses
- Attempts to reduce $\tan\delta$ and maximize the tunability $\Delta\varepsilon/\varepsilon$
- Development of a manufacturable process for deposition of STO films
- Integration of STO films with YBCO microwave resonators and filters to tune their frequency of operation while preserving a high $Q$
- Demonstration of a stand-alone 6-pole tunable filter system

## Technical Results

The first section of this report describes the low-frequency dielectric properties of the STO thin films we have grown by laser ablation and reactive coevaporation, and optimization of these properties. In the second section, we present results of our efforts to tune high-performance YBCO thin-film resonators with STO thin films while preserving the high $Q$ values.

## I. STO Thin Film Growth

### *A. Pulsed laser deposition*

We extensively studied the growth of STO thin films by laser ablation. We investigated the effect of growth conditions (substrate temperature, oxygen pressure, deposition rate, target density), doping, film thickness, annealing, substrates, and various layered structures on the materials properties and dielectric properties. For the purpose of tuning high-Q YBCO microwave filters, it is important to produce STO films with as low loss as possible, while maintaining a reasonable tunability. We found that this was accomplished most readily by depositing pure STO films on lattice-matched substrates under carefully identified growth conditions.

We measured the low-frequency (1 to 10 kHz) dielectric properties of our STO films by patterning coplanar interdigitated capacitor structures that were photolithographically defined using Au films. We also studied the effect on the loss of using *in-situ* metallization, YBCO electrodes, and structures designed to minimize the amount of superfluous electric field penetration into the STO films. We extracted the dielectric constants from the measured capacitance by modeling the electric field distribution of these structures.

Our measured temperature dependencies of $\varepsilon_r$ and $\tan\delta$ are similar to those reported in the literature, though we have been able to achieve very high dielectric constant values at low temperature (Figure 2). We observe an increase of both of these quantities with decreasing temperature until a temperature between 20 and 60 K is reached, at which point $\varepsilon_r$ and $\tan\delta$ reach a maximum and then begin to decrease. The initial increase has been attributed to softening of the soft optical phonon mode, and the subsequent decrease, seen only in thin films, may be due to the existence of a random internal electric field. We occasionally observe another loss peak occurring at approximately 100 K; this peak is in addition to the ubiquitous lower-temperature loss peak. For our films with higher dielectric constant values, however, this higher-temperature loss peak is usually absent. These peaks in $\tan\delta(T)$ are variously ascribed to phase transitions, though there is strong evidence that they are due to thermally-activated defect modes.

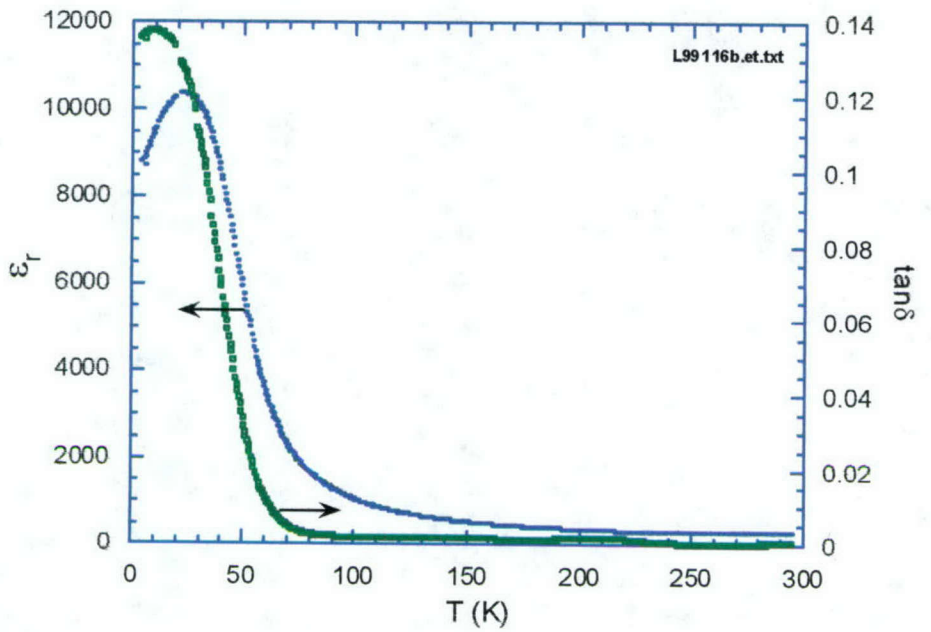


Figure 2. The temperature dependence of $\varepsilon$ and tan$\delta$ for a high- $\varepsilon$ STO film. This film exhibits a record high low-temperature dielectric constant for STO heteroepitaxial thin-film growth.

We primarily investigated the following substrate materials (with their respective lattice mismatches with single-crystal STO): $LaAlO_3$ (2.9%), MgO (7.9%), $NdGaO_3$ (1.9%), and $Al_2O_3$ (2.1%). We anticipated that the growth mechanism of STO may be different depending on the lattice match with the substrate; for example in the case of MgO, the formation of dislocations at the interface may serve to relieve the stress so that the bulk of the film grows with less stress and fewer defects. In fact, we found that we are able to grow the most satisfactory films on $LaAlO_3$ and $NdGaO_3$. It is much more difficult to deposit completely oriented films on MgO and $Al_2O_3$; care has to be taken not to nucleate (110) and (111) oriented grains. Furthermore, we always obtain lower values of $\varepsilon_r$ and tuning ($\Delta\varepsilon_r/\varepsilon_r$) on MgO and $Al_2O_3$. At least for laser-ablated films, then, these substrates proved unsatisfactory. And though the overall goal is to reduce tan$\delta$ and not necessarily to obtain high $\varepsilon_r$ values, we also find that the choice of substrate has little effect on the tan$\delta$ values for a given $\varepsilon_r$ value. However, we also studied the growth of STO on LSAT, which has an excellent lattice match to STO. While not leading to high $\varepsilon_r$ values, we found that growth STO on LSAT does allow us to obtain low loss values such that superior $k$ values can be realized. (See Figures 3, 12, 13.)

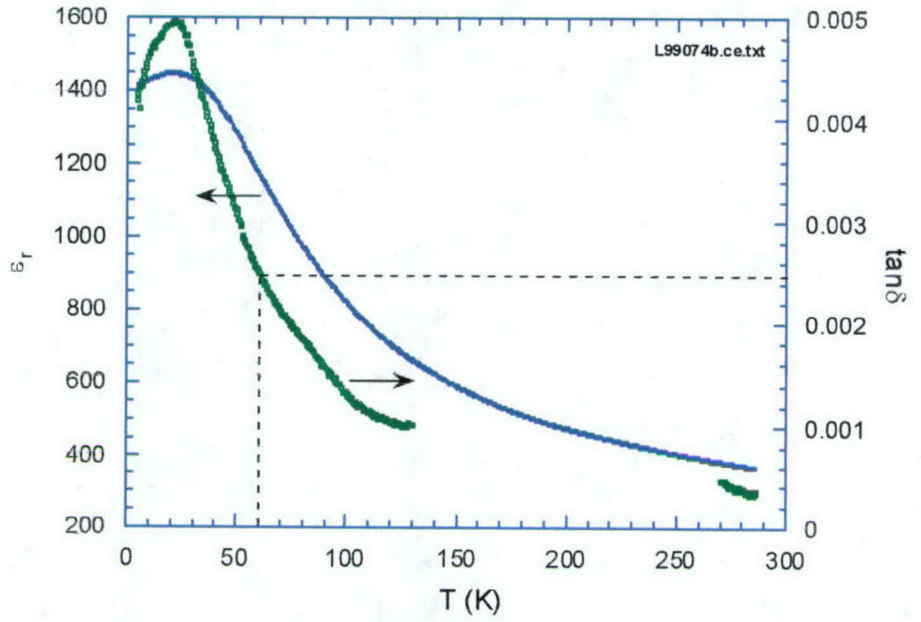


Figure 3. Temperature dependence of $\varepsilon$ and tan$\delta$ for an STO film on LSAT, demonstrating that at the typical operating temperature of 60 K, a low loss tangent value of 0.0025 is possible. Note that the low-temperature dielectric constant of this film is considerably lower than the example shown in Figure 2.

We additionally evaluated several buffer layers deposited between the substrate and STO film, which may also be expected to aid in stress relief or chemical/structural compatibility with the deposited film. We deposited the following materials as buffer layers: $LaAlO_3$, $NdGaO_3$, $SrRuO_3$, and $SrAlNbO_3$. (It is well known that $CeO_2$ – widely used as a buffer layer for YBCO films – leads to poor STO growth.) We deposited these buffer layers on each of the aforementioned substrates; note that in the case of $LaAlO_3$ and $NdGaO_3$, homoepitaxial growth is obtained, which has been reported to result in superior STO film growth. Unfortunately, we found that the addition of buffer layers usually results in poorer-quality films than sans buffer: we have never seen improvement upon adding a buffer layer, and usually the films were degraded.

### *B. Dependence on film thickness*

We found a relatively strong dependence of STO film dielectric properties on film thickness. Figure 4 displays the thickness dependence of $\varepsilon_r$ and tan$\delta$ for many STO films grown under different conditions and on various substrates, hence the range of values presented. Note a strong tendency for $\varepsilon_r$ to increase with increasing film thickness. Interestingly, we found this effect to abate above ~2.5 μm. The cause of any critical thickness is unknown. We speculate that as the films become thicker, the stress induced by the substrate is relieved, thereby leading to altered dielectric properties, perhaps due to reduced defect creation.

TEM investigations of our films have indicated nicely ordered growth from the substrate to the top of 2-μm-thick films, and they appear to be relatively free of extended defects throughout (see Figure 5). It is clear, however, that the film properties are altered as the films become thicker. However we do not believe that the films are becoming more "single-crystal-like" as they become thicker. Note in Figure 4 that as $\varepsilon_r$ increases with increasing thickness, so does $\tan\delta$. This is unlike single-crystal STO in which case $\varepsilon_r$ is higher than thin films, but $\tan\delta$ is lower. It is not possible to achieve STO single-crystal like properties in thin films.

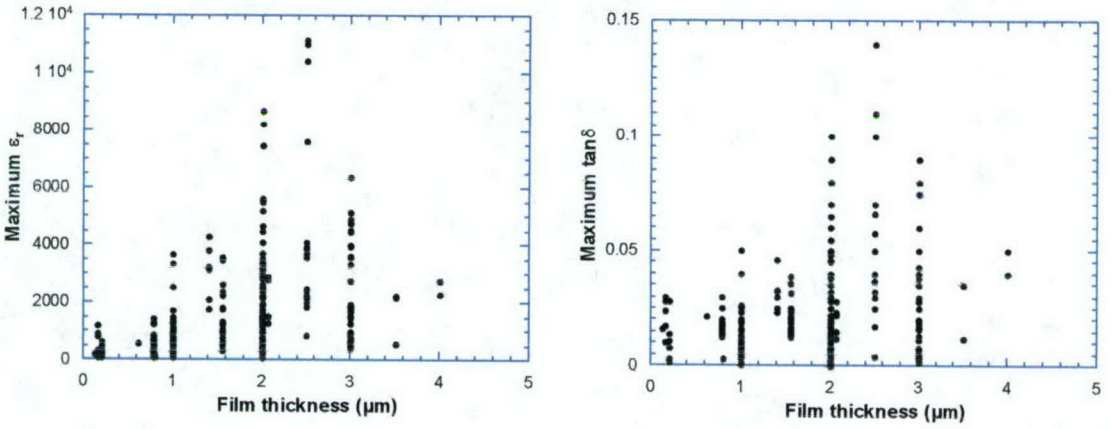


Figure 4. Thickness dependence of the maximum dielectric constant and maximum loss tangent for several PLD-deposited STO films.

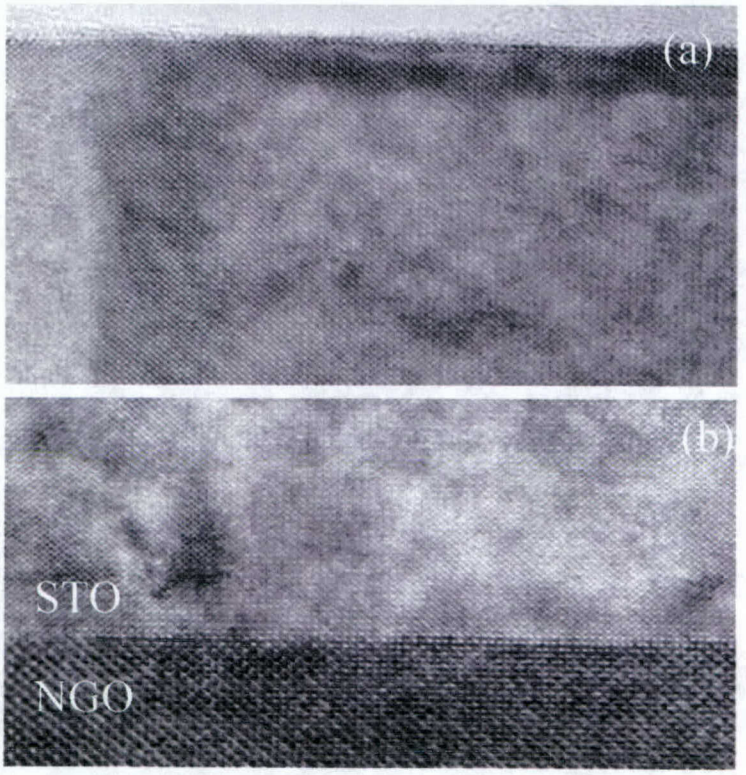


Figure 5. TEM image of an STO film deposited by PLD onto $NdGaO_3$. This film displays excellent crystallinity and very few defects, but at the interface (b) and at the top of the 2.5 micron-thick film (a).

### *C. Attempts to reduce loss*

We made a multitude of attempts to reduce the loss of our laser-ablated STO films. A summary of these efforts appears below.

- **Effect of growth conditions**
  - Effect of substrate temperature, oxygen pressure, and growth rate were studied

- **Substrate type and surface preparation**
  - Many different substrates were investigated (see Section A)
  - Various acid treatments and annealing protocols to alter the substrate surface were investigated.
  - Smooth and stepped surfaces studies
  - No clear effect on STO dielectric properties

- **Effect of film thickness**
  - See above, section B

- **Effect of composition**
  - Off-composition PLD and films targets were investigated
  - Microstructure of Sr- and Ti-rich films was studied by TEM
  - Best microstructure results from on-composition films

- **Effect of buffer layers**
  - See Section A

- **Elemental doping**
  - We made STO films doped with several elements of several different concentrations.
  - Dopants included Ce, Ca, Cr, Mo, Mn, W, Co, Y, Ga, Ir
  - Doping on both the Sr and Ti sites
  - The general effect was to reduce $\varepsilon$ and increase $\tan\delta$

We introduced a number of dopants, including Ca and Ce which presumably substitute for Sr, and Cr, Mo, Mn, and W which we expect to substitute for Ti. In addition, we attempted doping with Co, Y, Ga, and Ir. Only a small amount of doping on the Ti sites was necessary to dramatically alter the properties of the STO films. Doping the Sr sites produced less of an effect.

We found that doping produces several interesting changes in the dielectric properties of the films. However, the main effects of doping STO in all cases were a reduction in εr (without a significant improvement in tanδ), very often increases in tanδ, and degraded tunability of εr and tanδ. In addition, some dopants readily produced films which were weakly conducting, and in many cases the temperature dependencies of εr and tanδ were considerably altered. Despite the interesting behavior we observed, doping has not yet led to a reduction in tanδ and, in fact, has made things worse. We did not examine the microstructure of these doped films, so the implication is unclear; it is possible that our pure STO films are already as defect-free as possible.

- **Superlattices**
  - Several superlattice structures of STO/SAT and STO/SAN were made
  - $\varepsilon(T)$ and $\tan\delta(T)$ were altered, no reduction in $\tan\delta$

We made several attempts at reducing the loss by making superlattice thin film structures by forming repeated bilayers of STO and a lattice-matched dielectric with lower loss. We hoped this would lead to a reduction in the overall $\tan\delta$ of the films while preserving reasonable $\varepsilon_r$ values and tunability. We chose $SrAlTaO_3$ and $SrAlNbO_3$ as interlayer materials. These dielectrics are very well lattice-matched to STO and have low $\varepsilon_r$ and $\tan\delta$ values. X-ray diffraction spectra of these films displayed very clear

multiple satellite peaks, indicating excellent superlattice structure. Indeed, from these satellite peaks it was possible to calculate the thicknesses of the layers. We found that the temperature dependence of $\varepsilon_r$ and $\tan\delta$ is dramatically altered from pure STO films, and the peak in $\varepsilon_r$ and $\tan\delta$ shifts to higher temperatures as the interlayer thickness is increased. We do not understand the origin of this behavior. Increasing amounts of SAT also leads to a reduction in the overall dielectric constant, as we may expect. Unfortunately, we also observed that for a given dielectric constant, the superlattices have higher loss than pure STO films. Again, our attempt to reduce the loss had the opposite effect.

- **$O_2$ post annealing**
  - Low-$T$ anneals: $\downarrow \varepsilon$ and $\varepsilon\Delta/\varepsilon$, $\downarrow \tan\delta$
  - High-$T$ anneals: $\uparrow \varepsilon$ and $\varepsilon\Delta/\varepsilon$, $\uparrow \tan\delta$

- **Ozone post-annealing**
  - A dramatic change in dielectric properties was observed, but no improvement in the relationship between $\varepsilon$ and $\tan\delta$.

- **Deposition in ozone**
  - Films were deposited by PLD in an ozone ambient
  - No improvement in properties

### D. Reactive coevaporation

For purposes of producing STO films for production, a technique is desired which can grow films on large-area substrates with high throughput. Reactive coevaporation (RCE) is such a growth method, and we put considerable focus on growing STO films by this technique. We are the first group to grow STO films using reactive coevaporation combined with a rotating oxygen pocket heater, which we have used extensively to grow high-quality YBCO films. Using this technique, we are able to deposit STO on substrates that are up to 4 inches in diameter.

We determined the optimum RCE growth process windows for depositing STO films on $LaAlO_3$ and MgO substrates, in which case single-phase, epitaxial (100)-oriented STO films are readily obtained for the correct substrate temperature and oxygen pressure. This process window occurs in the range of 750 to 840 °C for $LaAlO_3$ and 810 to 840 °C for MgO, with a minimum oxygen pocket pressure of 20 mTorr. We also investigated the growth of STO on other substrates such as LSAT, r-plane sapphire, m-plane sapphire, and YSZ. In the case of LSAT, which is closely lattice matched to STO, we are also able to obtain (100)-oriented STO films for temperatures between 750 and 800 °C. For r-plane sapphire, we obtain only (111)-oriented STO films under all growth conditions. Similarly for growth on

YSZ, we also observe (111)-oriented STO films. For m-plane sapphire on the other hand, we thus far have observed only very weak (110) reflections in the $2\theta$ x-ray scans. Interestingly, the dielectric properties of our (111)-oriented STO films are not substantially different from those measured on (100)-oriented films; values of dielectric constant, loss, and tunability are similar. This may be a consequence of our measuring geometry (coplanar interdigitated electrodes), which samples different directions of the film cross-section due to the nonuniform electric field distribution. It may be possible to obtain (100)-oriented STO on these substrates using a suitable buffer layer, but this is not within the scope of the FAME program.

We found that the closely lattice matched substrate LSAT does easily allow the formation of high-quality, well-oriented (100) STO thin films by RCE. To date, the dielectric properties of these films--as opposed to those deposited on LSAT by PLD--do not indicate that this substrate is superior to LAO, MgO, or NGO for films grown by RCE.

Also unlike PLD, for which the composition of the target is generally reproduced in the deposited film, the composition of RCE films can be readily adjusted by changing the deposition rates of Sr and Ti. Although the necessary monitoring of these rates is discussed below, we mention here that accurate compositional measurement of the STO films is crucial in order to have appropriate feedback into the deposition process. Over the course of this project, we developed an in-house EDX capability for compositional measurement.

### *E. RHEED monitoring*

While the RCE technique affords flexibility over film stoichiometry for the purpose of studying the effect of composition on dielectric properties, it is also far more difficult to control composition by this technique than by laser ablation. Figure 6 displays the sensitivity of the dielectric properties to composition for RCE-deposited films. In addition, the difficulty of reproducibly controlling the stoichiometry is exacerbated by our occasional desire to grow quite thick STO films, which have higher dielectric constants and superior tunability. In this case, rate monitors such as quartz crystals and atomic absorption tend to saturate or drift during the run, and maintenance of the correct film composition can be problematic.

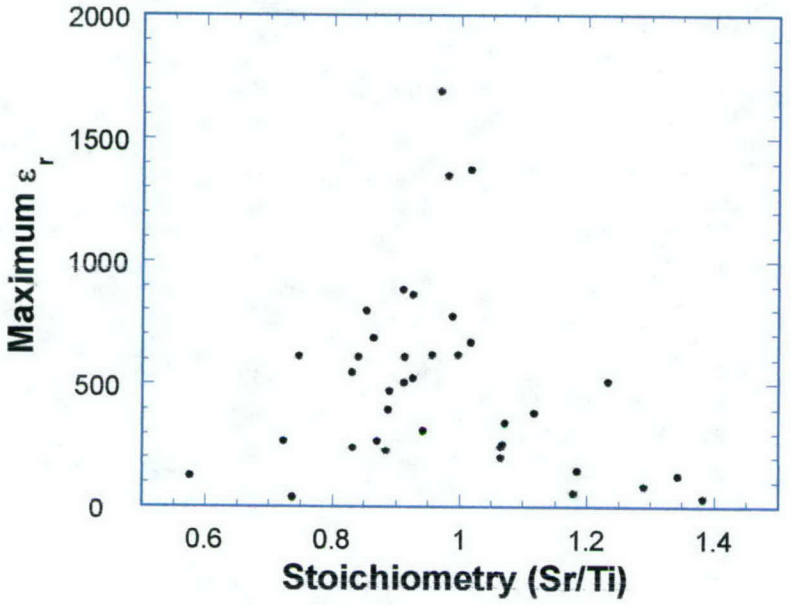


Figure 6. Maximum low-temperature dielectric constant as a function of stoichiometry for several RCE-deposited STO films. The composition was measured by EDX.

Thus during the course of this work, we developed a reflection high-energy electron diffraction (RHEED) procedure to help control the film composition during the run. The principle is that the RHEED image obtained from the growing STO surface provides information on the lattice spacing during deposition. We know that the room-temperature lattice constant of our STO films depends on stoichiometry, and we assume a similar relation holds at the deposition temperature. Thus by controlling the Sr and Ti rates to maintain particular lattice spacing during the run as indicated by RHEED, we can control the stoichiometry. We found that we can readily detect a lattice constant change of 0.1% by this technique. This allows small changes in stoichiometry to be detected within just a few unit cells of altered composition.

We found that the use of RHEED leads to a distinct improvement in the crystallinity of our STO films, which is due to improved compositional control. Figure 7 displays the FWHM values of the rocking curve peak for the STO (200) x-ray line for a variety of STO films. It is readily apparent that this value improves significantly with the introduction of RHEED compositional monitoring. The FWHM of the (200) line itself behaves similarly.

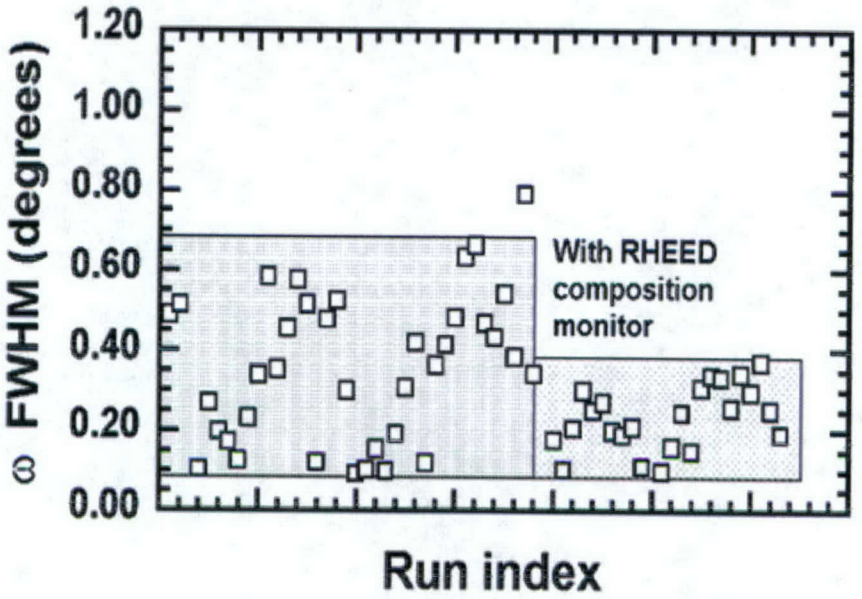


Figure 7. Improvement of the STO (200) x-ray rocking curve width when using RHEED as a composition monitor during growth. The graph illustrates that improved compositional control results in superior film crystallinity.

We also further extended this technique to perform a real-time observation of strain relaxation during *in-situ* growth of STO thin films by measuring the in-plane lattice constant at the film surface using RHEED. The initial misfit strain in the STO film is tensile on MgO and compressive on $LaAlO_3$, as expected from the lattice mismatches between the film and the substrates (see Figure 8). We find that strain relaxation begins immediately after the deposition starts, but is not complete until the film thickness reaches 500 – 2500 Å depending on the substrate and the deposition temperature. The strain relaxation at the growth temperature influences the film strain at room temperature, which is compressive for both substrates for thin STO films.

The *in-situ* RHEED measurement during STO film growth reveals that, although the critical thickness is very small on both LAO and MgO substrates, the complete misfit strain relaxation does not occur until the film thickness reaches 500 – 2500 Å. The film strain at room temperature is influenced by the strain relaxation at the growth temperature through misfit dislocations. In thin films with high densities of misfit dislocations, an increased compressive strain is found for both substrates despite the differences in their lattice and thermal expansion mismatches with STO.

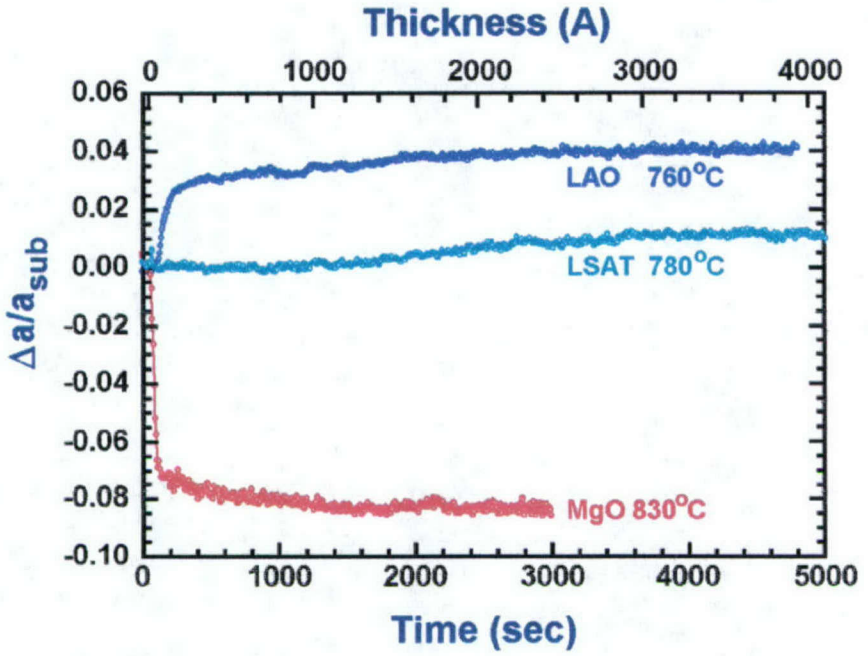


Figure 8. Real-time strain relaxation measured by *in-situ* RHEED for STO films grown on LAO, LSAT, and MgO substrates. The y-axis displays the lattice constants of the growing STO film as a percentage difference relative to the substrate lattice constant value at the indicated temperature.

### *F. Optimization of tuning and loss*

As already mentioned, we demonstrated the PLD growth of heteroepitaxial STO films with extremely high values of dielectric constant ($>10^4$) and tunability (up to a factor of 20) at low temperatures. However, the loss tangent tends to scale with permittivity, so these films are not necessarily the most desirable for high-Q applications. It then becomes necessary to select STO films with low values of $\tan\delta$ and reasonable tuning. The figure of merit, $k$, is often used to describe the relationship of tunability to loss, and is given by

$$k \equiv [\varepsilon(0)-\varepsilon(E)]/[\varepsilon(0)\tan\delta(0)],$$

where $E$ is the electric field. Here we used the zero-field $\tan\delta$ value, which represents the worst-case value (i.e., the highest loss).

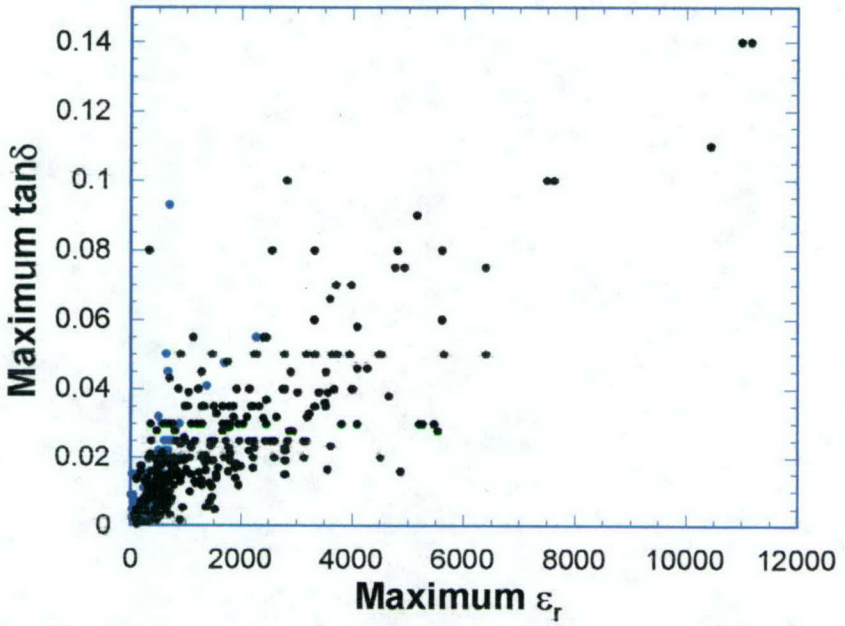


Figure 9. Dependence of the maximum loss tangent on maximum dielectric constant for many PLD- and RCE-deposited STO films.

We observed a general trend for the loss, tan$\delta$, to depend on the dielectric constant as shown in Figure 9, which gives measurements for both RCE and PLD STO films. Figure 10 shows, similarly, that the loss and the tunability are also linked. The result of studying all the effects discussed above was to allow us to grow films which lay along the lower portion of the curve, i.e. to produce films that minimized the loss for a given tunability. We then selected growth conditions that gave us films with an acceptable tan$\delta$, but not having maximum tunability (see Figures 12 and 13). Also note that our intended temperature of operation is 60 to 70 K, not at the low temperatures of 10-20 K where the loss peak occurs and the loss is greatest. Thus the data in Figures 9 and 10 represent the upper bound on the loss; at our operating temperatures it can be much less, as demonstrated in Figure 3. In fact as shown in Figure 11, the highest *k* factors are not obtained for the films with the largest dielectric constant (and those consequently having the greatest tuning). Due to the wide range of loss tangents we are able to produce--over nearly two orders of magnitude--the *k* value is quite sensitive to the loss for our films. Figure 11 shows that lower loss films lead to higher *k* values, even though they demonstrate less tuning at a given field. The solution for integration with high-Q HTS filters, particularly since the loss decreases with applied voltage, is to choose lower-loss films and operate at a higher applied voltage. This is the approach we have taken in implementing our tunable filters.

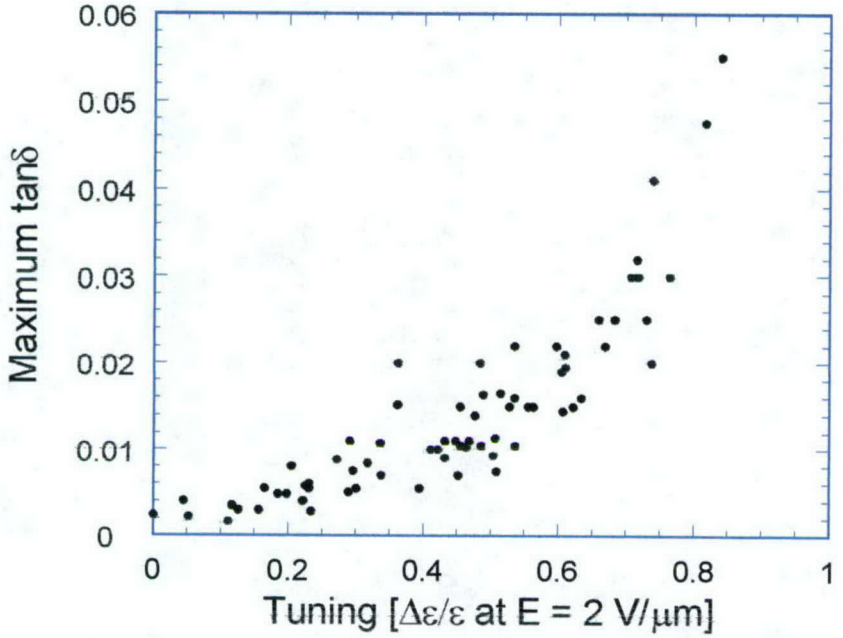


Figure 10. The relation between the maximum loss tangent and tunability for an applied field of $E$ = 2 V/micron for several STO films deposited by RCE.

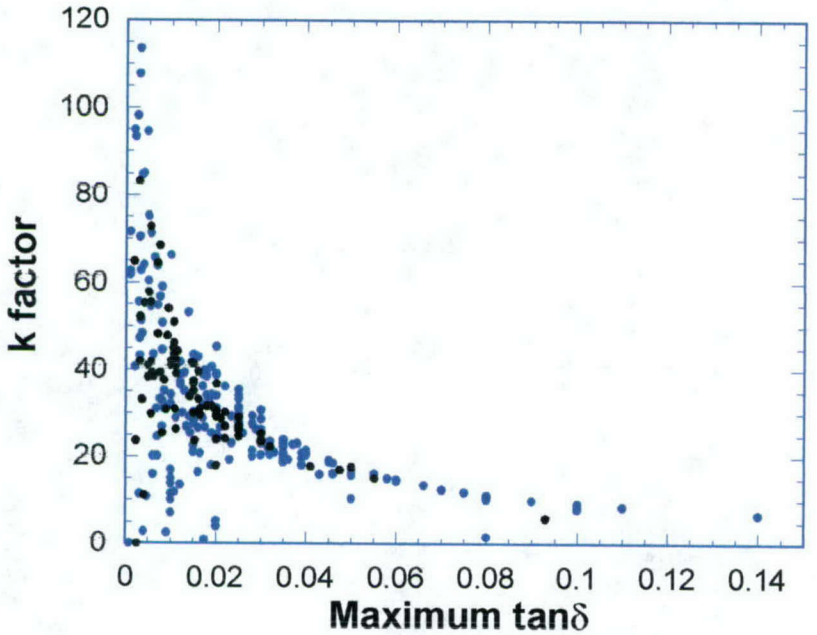


Figure 11. The dependence of the figure of merit, $k$, on maximum loss tangent for many STO films deposited by PLD and RCE.

Figure 12 shows the electric-field dependence of $\varepsilon$ and $\tan\delta$ for a low-loss STO

film. This figure demonstrates that STO films with relatively low values of loss tangent but with acceptable tuning may be obtained at temperatures of interest for applications. This measurement was made at 10 kHz by patterning a Au interdigitated capacitor on top of the film. Both quantities decrease with applied field as expected. We have found that this decrease continues to occur with substantially higher field values, meaning that for high-Q operation, it is desirable to operate the STO capacitors in a high-voltage regime.

Figure 13 displays the figure of merit for this film as a function of average electric field (with fixed $\tan\delta$ value). Such *k*-values are among the highest reported in the literature. The dielectric constant of this film is not especially high, even at this temperature. It is relatively easy to grow films with values ten times this value at this temperature, but the loss is higher, and *k* is lower, as shown in Figure 11., emphasizing the importance of tailoring the film properties for applications.

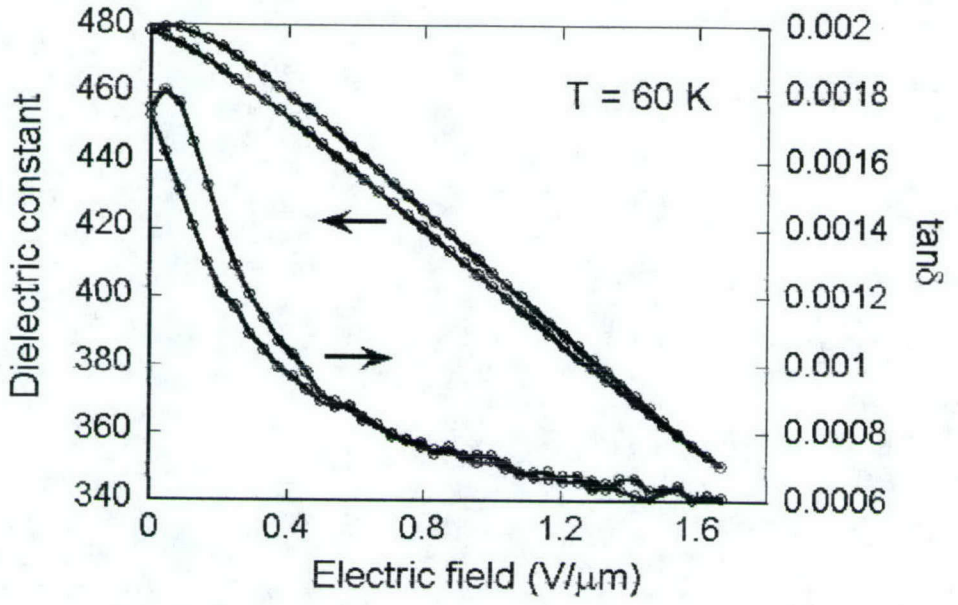


Figure 12. Dependence of dielectric constant and loss tangent on electric field for an STO film with a relatively low permittivity and low loss, measured at 10 kHz. The tunability in this modest field is $\Delta\varepsilon/\varepsilon$ = 27%. Note that this performance is actually better than single-crystal STO, which, despite its lower loss, displays virtually no tuning at this high temperature.

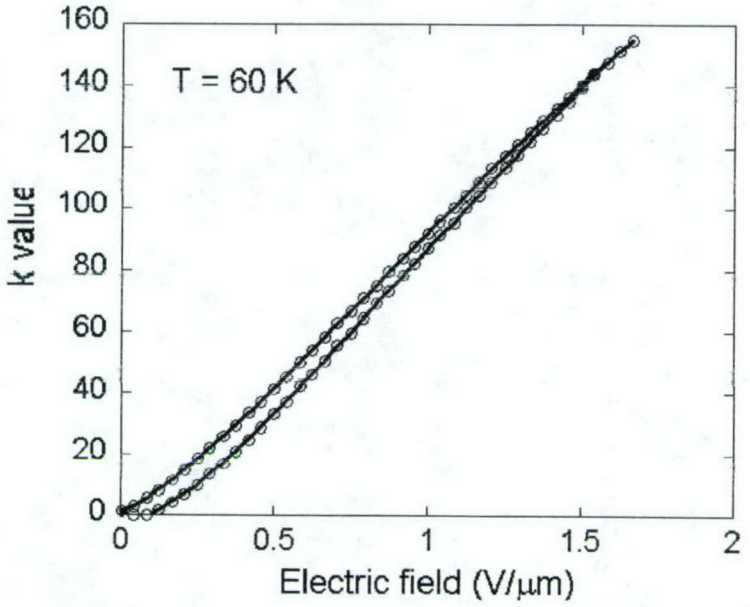


Figure 13. The figure of merit $k$ as a function of applied electric field for the STO film in Figure 12. The figure of merit is defined in the text. Note that the zero-field value of $\tan\delta$ is used in this definition.

## II. Integration with YBCO Resonators and Filters

The second major challenge of our FAME program was how to integrate our optimized STO thin-film capacitor structures with our high-performance HTS thin film resonators and filters. We explored a wide variety of integration schemes and resonator and filter designs. We studied both the physical methods of attaching our STO films to the circuits and coupling them to our resonators, and we explored various coupling design schemes. We used these circuits to simultaneously determine their suitability for applications and to evaluate the RF properties of our STO thin films. We will discuss some highlights of our work.

We also measured the dielectric properties of our STO films up to 40 GHz by making broadband coplanar waveguide measurements in collaboration with colleagues at NIST. Another group at NIST also made cylindrical cavity RF measurements of our films. We additionally carried out experiments that placed an upper bound on the tuning speed of our circuits. These topics will not be discussed in this report.

### *A. Flip Chip Configuration*

Although the tunability of our STO films can be very large, the high loss tangent of these films in relation to the very high Q of YBCO microwave circuits requires us to decouple the tunable STO capacitor portion of the circuit from the YBCO

resonator part. We initially accomplished this by fabricating the STO capacitor on a separate chip (as already described), which allows us to optimize its dielectric properties, for example, by using different substrates than that used for YBCO, and by employing optimal growth conditions. Once the interdigitated capacitor structure was patterned on top of the STO chip and the chip subsequently diced into a small structure so as to minimize the amount of STO, we initially mounted these chips to our package and wirebonded them to our HTS circuits. However, the additional loss contributed by our metal wires proved to be excessive. As a result, we began flip-chipping our STO capacitors directly onto our HTS circuits. These STO capacitors were placed onto the YBCO microwave circuit wafers in a location that is weakly coupled via YBCO lines to the resonator for the purpose of tuning its center frequency. This flip-chip configuration allowed us to quickly determine the performance of various STO thin film capacitors for the same YBCO resonator or filter circuit.

An example of one of our lumped-element YBCO resonator designs is shown in Figure 14. The interdigitated capacitor structure is evident, as is the line around its perimeter which provides the inductance for this LC resonant circuit. These resonators have center frequencies of ~850 MHz. The input and output coupling ports are shown at the left and right sides of the circuit. The part of the circuit at the lower left is where the STO flip is attached. One side of the STO capacitor goes to ground, and the other side is coupled into the resonator via a solid YBCO line. This is our "strongly-coupled" circuit, for which the STO capacitor loads the circuit considerably, thereby reducing its *Q*. This circuit allowed us to determine the maximum tunability of the resonator for different STO materials. In addition, this circuit was modeled quite well, so that we could use it to extract the loss tangent values of our STO films at these high frequencies.

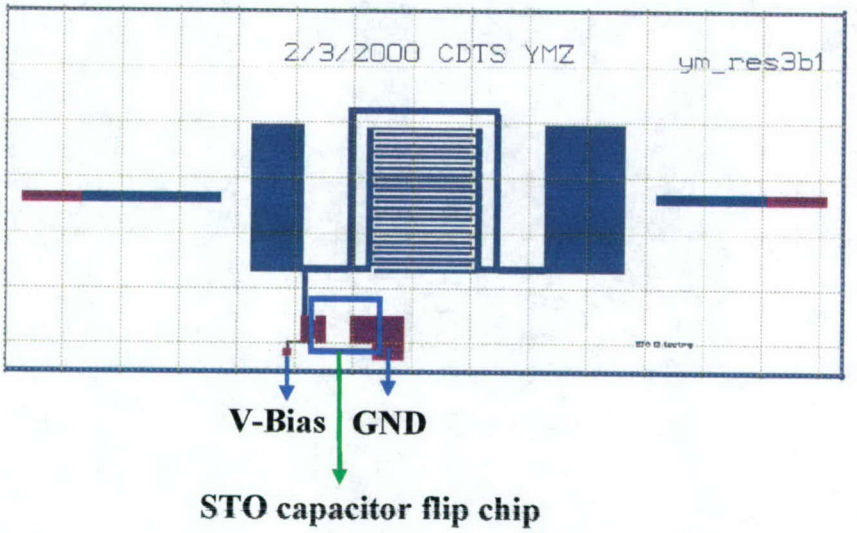


Figure 14. Layout of a thin-film YBCO lumped-element resonator with a strongly-coupled STO tuning capacitor (STO flip chip goes in the gap of the bottom circuit).

The representative performance of this circuit is shown in Figure 15, which shows the tuning of the *Q* and center frequency $f_0$ of the resonator at 77 K as a function of the voltage applied to the flip chip STO capacitor. Note that as voltage is applied and the loss tangent and capacitance of the STO are altered, the loaded *Q* of the YBCO resonator increases and its center frequency also increases. The center frequency of the resonator can be changed by ~7 MHz even for this modest applied voltage. Even though the loaded *Q* increases with *V*, its value is unacceptably low for our applications, reaching in this case about 4460 at 40 V. From this measurement, we are able to extract the Q value for this STO film: The *Q* of 444 at 40 V correlates to a loss tangent of ~ 0.002 at this frequency of 829 MHz, indicating the high quality of our STO films.

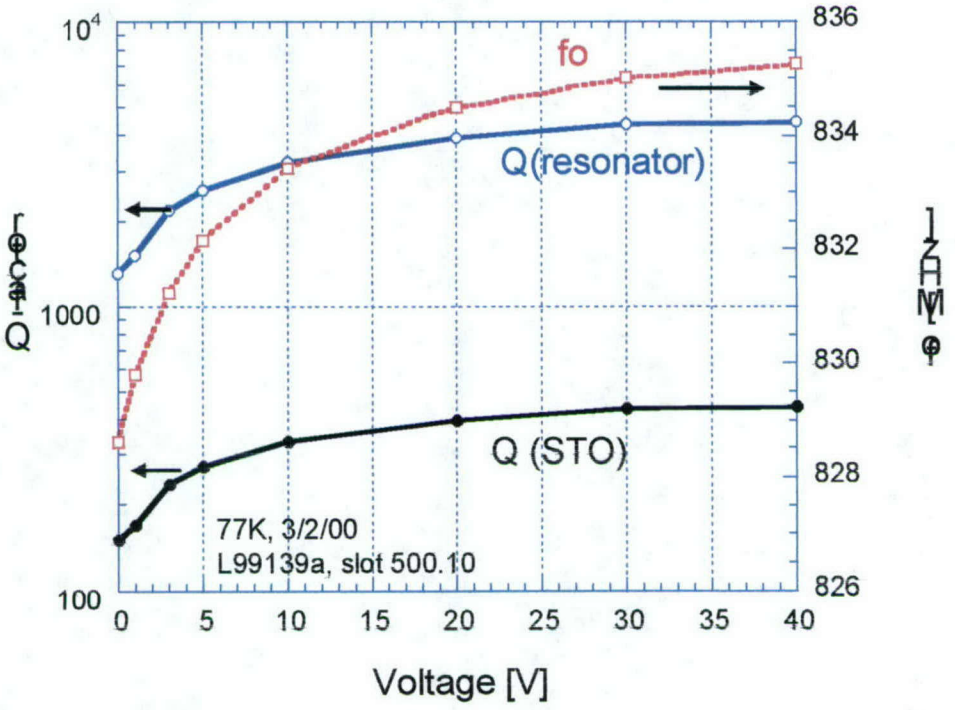


Figure 15. Dependence of *loaded Q* and center frequency $f_0$ of a lumped-element YBCO resonator with a strongly-coupled STO thin-film capacitor. As the applied DC voltage is increased from 0 to 40 V, *Q* increases, and the center frequency is tuned by about 7 MHz. Also shown is the extracted *Q* of the STO capacitor, indicating a reasonable tan$\delta$ of our material at these frequencies.

### *B. Monolithic configuration*

For manufacturing purposes, and to reduce the loss due to normal metal

contacts and electrodes, it may be desirable to deposit the STO thin film and YBCO film on the same substrate, and pattern the chip in such as way to make a tunable microwave circuit. With the RCE technique, this may be performed for large-area substrates of 2" in diameter or greater.

As already mentioned, it is necessary for the STO portion of the circuit to be physically decoupled from the YBCO resonator. In the monolithic approach, we accomplished this by either depositing the STO through a shadow mask, or by etching away most of the STO film except the area where the interdigitated STO capacitor will be formed. The first approach could, in principle, be accomplished *in situ*, while the second requires an intermediate processing step. Whichever approach is taken, it is critical to form shallow ramp edges on the STO, such that deleterious grain boundaries are not formed in the overlying YBCO film. The YBCO film is then deposited on top and patterned to form the electrodes for the STO capacitor, the coupling leads, and the microwave circuit.

Generally, we have had more success with the etching approach. We are not sure if the shadow mask technique leads to poor quality STO, or whether contamination of the substrate surface is the problem, leading to a poor quality YBCO film. Figure 16 is a photograph of a portion of a monolithic tunable resonator made by the etching technique. The rectangle of STO left after etching can be seen in the lower central part of the picture. Elsewhere is the underlying MgO substrate and overlying YBCO circuit. The behavior of these devices is not as consistent as we would like; however it approaches the performance of our flip-chip circuits. For a resonator with a center frequency $f_0$ greater than 1 GHz, we are able to tune $f_0$ by a few MHz with an applied voltage of 100 V for Qs of a few thousand. For higher-Q resonators--over 12,000 or so--we can tune a fraction of a MHz using this monolithic design.

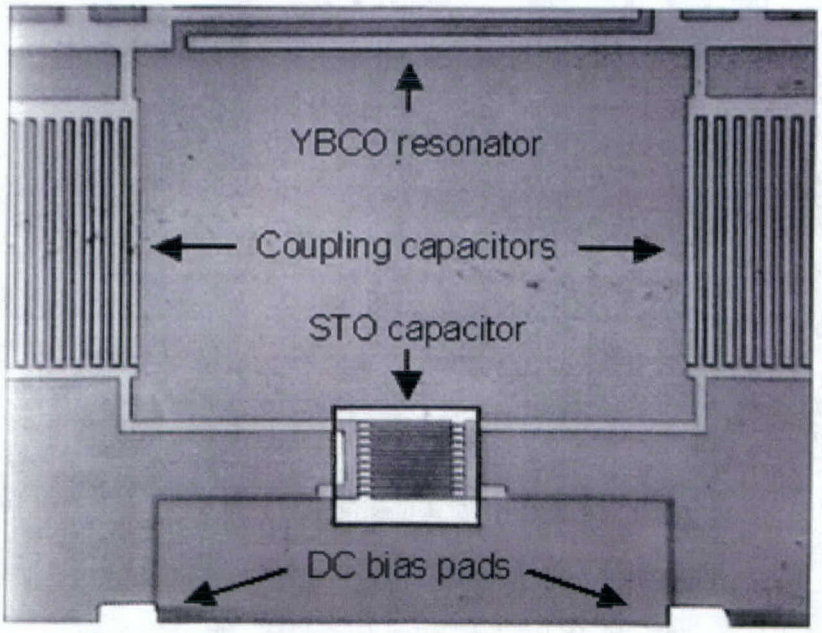


Figure 16. Photograph of a portion of a monolithic tunable resonator, in which STO and YBCO are deposited on the same substrate. The bright rectangle is the STO thin film; all other lines are YBCO. The width of the STO patch is 550 μm.

### *C. Effect of coupling*

The degree to which the STO portion of the circuit is coupled to the YBCO resonator naturally determines the Q that is attainable. We measured the effect of coupling by changing the value of the coupling capacitors between the STO capacitor and the YBCO resonator. This can be done on a single circuit by destructively removing portions of these capacitors to lessen their value. Figure 17 shows the lumped-element tunable resonator design we have used to investigate the effect of coupling. Again, the portion of the circuit on the bottom is where the STO flip chip is attached. We found that this symmetric design provided better performance compared to the asymmetric design of Figure 14. The rectangular YBCO blocks connecting the STO flip chip to the YBCO resonator are actually capacitive coupling banks. The resolution of the figure as reproduced here is not sufficient to see the interdigitated fingers making up these coupling capacitors. By laser scribing the fingers of these banks, we thereby can alter the strength of the coupling of the STO flip chip to the resonator circuit.

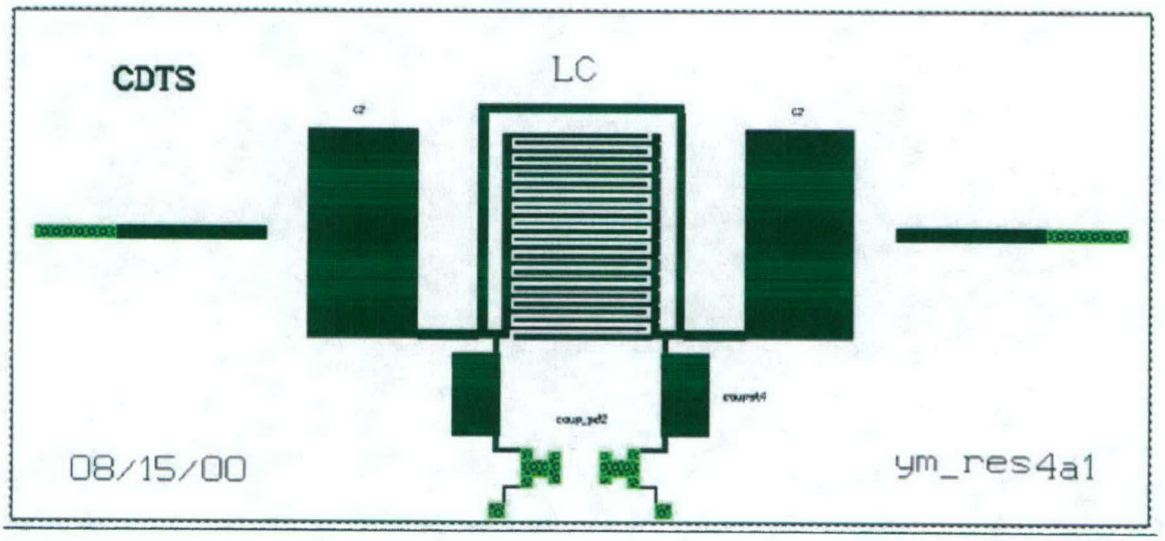


Figure 17. The tunable lumped-element resonator circuit used to explore the effect of coupling to the STO flip chip.

Figure 18 displays the performance of a flip-chip tunable resonator circuit for different coupling values. Each set of points represents the range of tuning of $Q$ and $f_0$ for applied voltages of 0 to 80 V. Note first that the center frequency of the resonator changes as the coupling changes, moving to higher frequency as the effect of the STO capacitance lowers.

For relatively strong coupling, the $Q$ is rather low, but the tuning range is relatively large. This can be seen for the data in the lower left portion of the figure, for which a $Q$ of 500 to 1200 is attained for a tunability of $\Delta f_0$ = 10 MHz. The detailed behavior of $Q$ and $f_0$ is shown in the inset. Moving toward the right of Figure 18, the coupling is made successively weaker. It can be seen that the $Q$ of the resonator improves and the tuning range decreases as the coupling is decreased. For relatively weak tuning, for example, a $Q$ value above 20,000 is attained at the expense of a much smaller tuning range, $\Delta f_0$ = 0.25 MHz.

Figure 18 illustrates the range of performance that we were able to achieve. It is possible to maintain a loaded $Q$ over 25,000 while allowing a high-performance YBCO microwave filter to be trimmed electrically. Wide-range electrical tuning (i.e., tuning $f_0$ by a significant percentage), is not possible by this technique due to the loss tangent of the STO. However, as noted earlier, $Q$ continues to improve and $f_0$ continues to change as we apply higher voltages. Thus for our tunable filter work, we explored the possibility of working at much higher relative voltages in order to obtain high $Q$ and acceptable tunability.

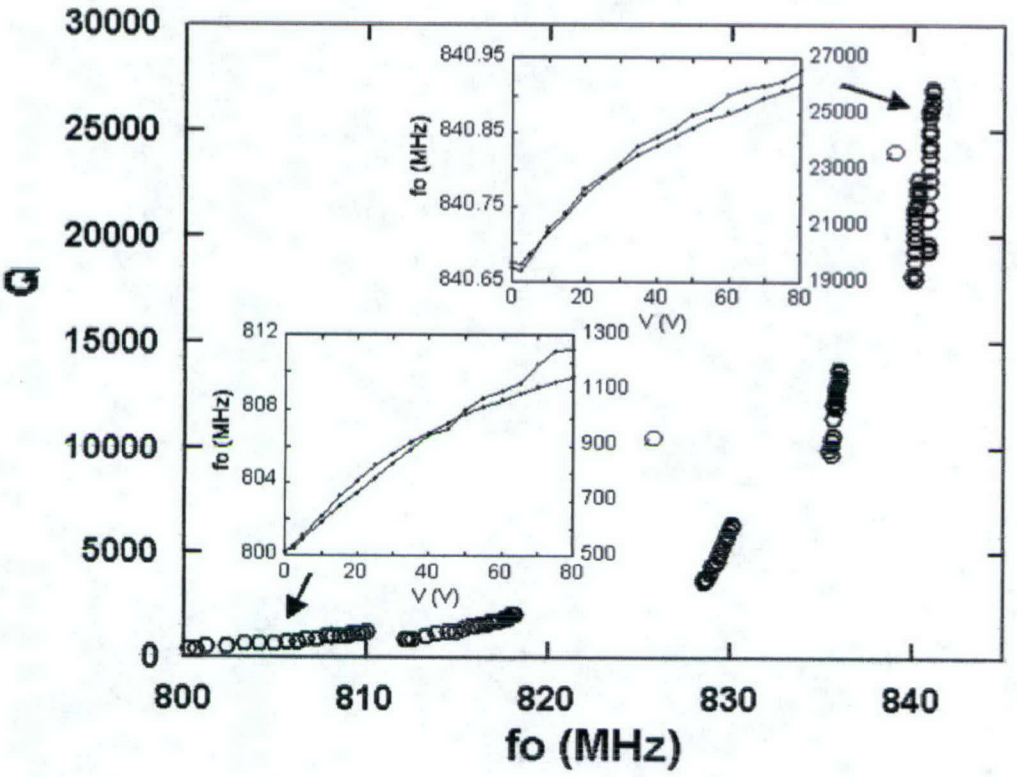


Figure 18. Quality factor vs. center frequency for an STO-tuned YBCO resonator with different coupling values. There are six sets of data points, each of which represents the value of $Q$ and $f_0$ as the DC bias is changed from 0 to 80 V. The insets show details of the response of $Q$ and $f_0$ in the weak and strong coupling regimes; dashed lines represent $Q$ and solid lines are $f_0$. For weak coupling, $\Delta f_0$ = 10 MHz, and for strong coupling, $\Delta f_0$ = 0.25 MHz.

### *D. High frequency resonators*

We also designed and fabricated a number of higher-frequency YBCO ring resonator circuits, as described in previous reports. We coupled STO to these structures using a flip chip approach and measured their performance and tunability. We were also able to extract the Q values of the STO films at these frequencies. The results of some of these measurements are summarized in Table I. It can be seen that significant tunability of these high frequency resonators could be achieved at modest Q values. Also, the extracted $Q$ and $\tan\delta$ values of our STO films show good performance.

Table I. Summary of tunable high frequency YBCO ring resonator results.

| $f_0$ | Q | Tuning at 40 V | $Q_{STO}$ | tan$\delta$ |
|---|---|---|---|---|
| 6.76 GHz | 959 | 6 MHz | 1136 | 0.001 |
| 12 GHz | 1201 | 14 MHz | 916 | 0.001 |
| 13 GHz | 943 | 46 MHz | 238 | 0.004 |

### *E. Tunable six-pole filter*

We previously reported the performance of a tunable two-pole YBCO filters. Here we discuss our demonstration of a six-pole tunable bandpass filter. Since the performance of a six-pole YBCO filter is generally sufficient to be useful in telecommunications applications, we were eager to determine the performance that can be achieved with tuning enabled by STO. We designed, fabricated, and tested a six-pole capacitively-coupled YBCO tunable bandpass filter which is 2 MHz wide centered at about 795 MHz. Each filter was fabricated using double-sided YBCO films on $LaAlO_3$ substrates. Six thin-film STO flip-chip capacitor dies are used as tuning elements; each capacitor tunes the center frequency of the corresponding resonator. Figure 19 shows the layout of out six-pole tunable filter. The six resonators are readily apparent, and the location of the flip-chip STO capacitors is indicated. This filter was patterned on one half of a 2" double-sided wafer. Figure 20 displays a photograph of the tunable filter when mounted in its cryopackage.

Figure 21 displays the response from our initial tuning tests for this filter. The voltages applied to the STO capacitors to tune the filter are indicated in the legend. For this filter operating at 60 K, we achieved a frequency slope of 83 dB/MHz and a rejection of 60 dB at 2 MHz from the band edge. The insertion loss is higher than a YBCO filter without tuning capacitors, but it remains below 2 dB. Note that as voltage is applied, the filter response is tuned to higher frequencies as expected, and the insertion loss improves due to the Q improvement of the STO. For applied voltages of 200 V, we are able to tune this

filter by nearly 1 MHz.

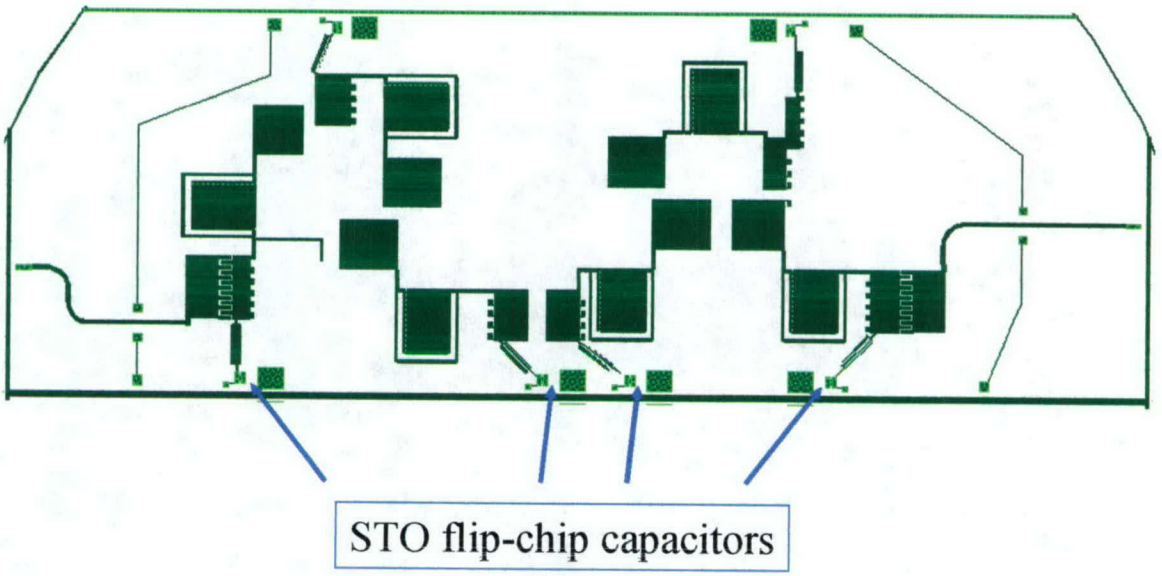


Figure 19. Layout of our six-pole tunable HTS filter. The location of the STO flip-chip capacitors is shown.

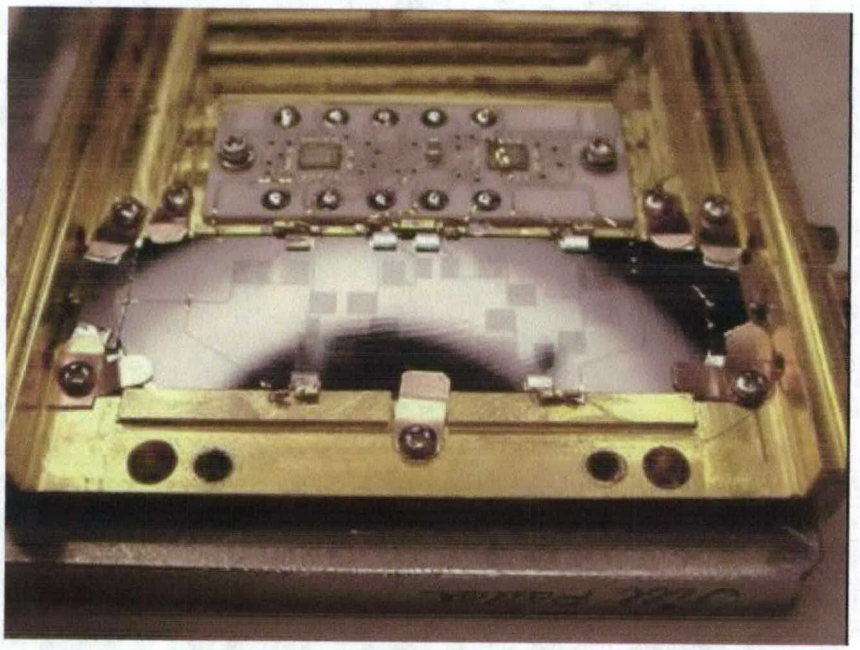

Figure 20. The six-pole filter mounted in a cryopackage for testing.

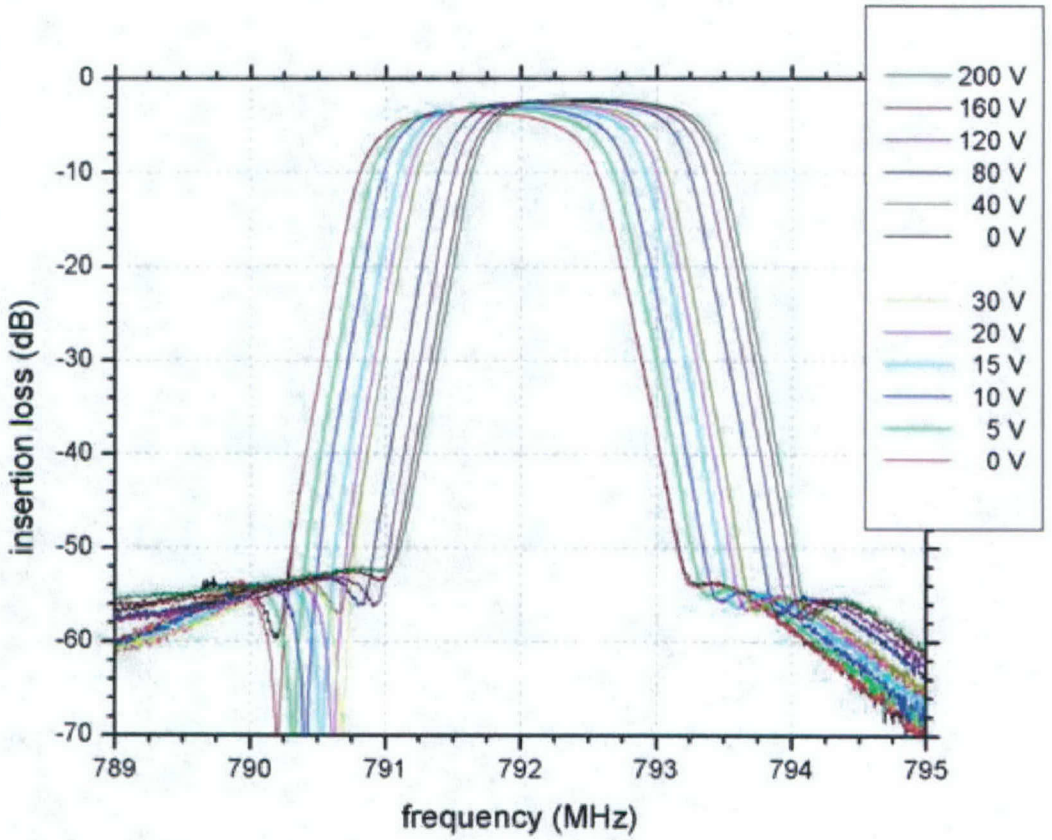


Figure 21. Initial measurements of the tunability of our six-pole tunable HTS filter. The bias voltages applied to the STO capacitors to tune the individual poles are shown in the legend. The zero-voltage response of the filter is adequate, with steep sloped, and a rejection of nearly 60 dB, 2 MHz from the band edge. Note, however, that the insertion loss is just under 2 dB. As voltage is applied to the capacitors, the frequency response changes, and the insertion loss improves.

Subsequent to demonstration of this tunable filter, we worked on development of a completely stand-alone electrically tunable six-pole filter system, with auto tuning. The tuning algorithm was developed to apply voltages to each STO tuning element individually and incorporated a lookup table so that a specific frequency range could be typed into the computer so the filter response would be automatically adjusted accordingly.

The applied voltage range in this case extended to several hundred V, with a maximum available voltage of 700 V. Figure 22 displays the response of this 6-pole filter for a range of voltages applied by the tuning algorithm. Note that the filter response improves considerably as it is tuned over a range of over 1 MHz. The out-of-band rejection remains better than 50 dB over the entire tuning range; as the filter is tuned, the sharpness of the corners improves, indicating an improvement in *Q*. Also, as the filter is tuned, the insertion loss improves to well under 1 dB. The high performance and tunability of this filter represent the state-of-the-art for electrically trimmable, multipole, high-*Q* filters.

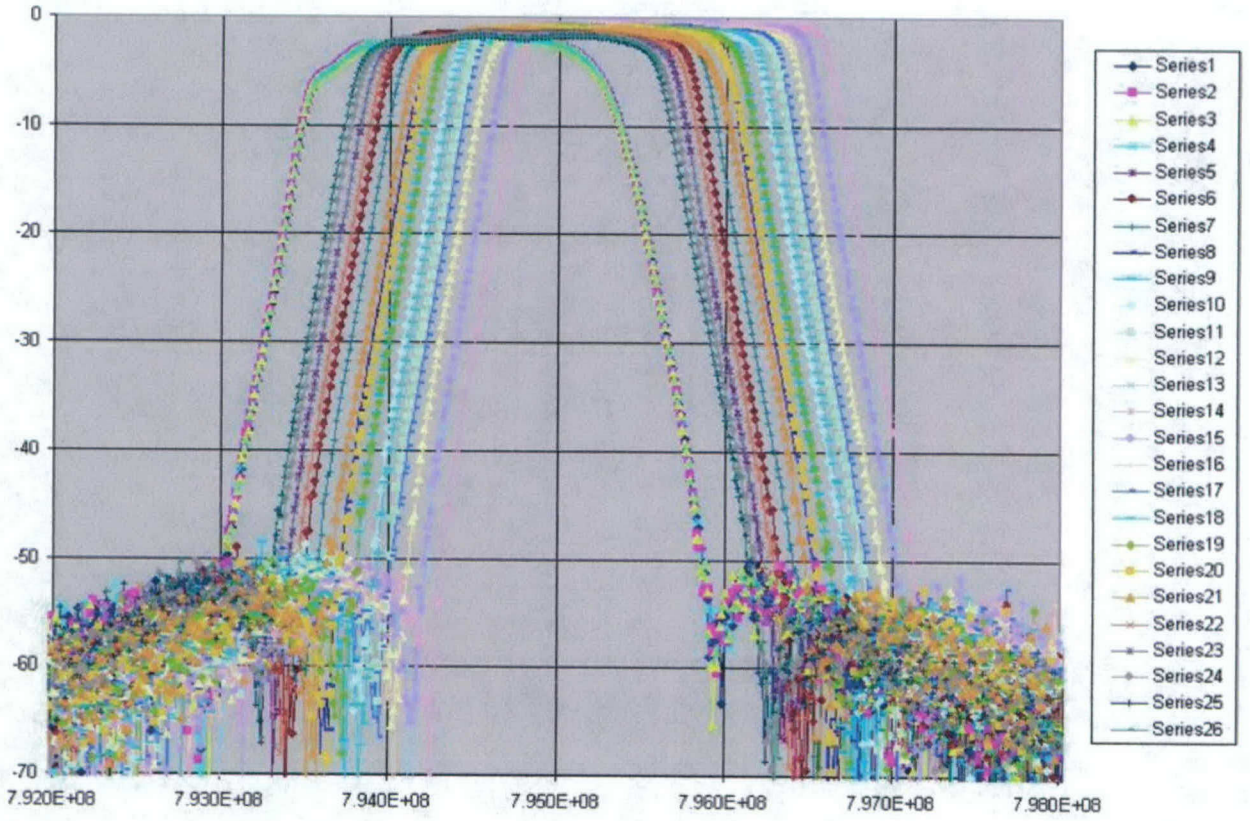


Figure 22. Response of a stand-alone, auto-tuned, six-pole filter demonstration. For applied voltages of several hundred V (each STO element is tuned differently), the filter response is tunable over a range greater than 1 MHz. The filter response improves considerable as it is tuned, with the insertion loss remaining under 1 dB for higher applied voltages.

## Implications for Further Research

Our work on this FAME program has demonstrated the feasibility of integrating tunable dielectric thin film materials with high-performance HTS thin filters in order to electrically tune their response characteristics. These studies have also highlighted the possibility of making further improvements in such electrically tunable filters by additional research in the following areas:

- Growth studies of STO thin films and new tunable dielectric materials and structures
- Investigations of lower-loss tuning structures
- Investigations of defects in tunable dielectric thin films and their effect on the dielectric properties and tunability
- Further research into understanding the extrinsic loss mechanisms of these thin films

- Additional studies of advanced and novel filter designs incorporating tunable dielectric elements with high-performance HTS microwave filters to exploit the tuning/loss tradeoff

## Special Comments

Additional details of the work discussed here can be found in the following publications:


1. B.H. Moeckly and Y.M. Zhang in MRS Proc. **603**, ed. by Q. Jia, F.A. Miranda, D.E. Oates, and X. X. Xi , pp. 45-56 (2000).
2. B.H. Moeckly and Y.M. Zhang, IEEE Trans. Appl. Supercond. **11**, 450 (2001).
3. L. S.-J. Peng, N.F. Heinig, and B.H. Moeckly, Mat. Res. Soc. Symp. Proc. **688**, 211 (2002).
4. B. H. Moeckly, L.. S.-J. Peng, and G. M. Fischer, IEEE Trans Appl. Supercond. (2003).
5. Luke S.-J. Peng, X. X. Xi, and Brian H. Moeckly, Appl. Phys. Lett. (2003).
6. L. S-J. Peng and B. H. Moeckly, J. Vac. Sci. and Tech. (2004).
7. G. M. Fischer and B. H. Moeckly, unpublished.